Journal of Applied Physics ARTICLE scitation.org/journal/jap

Differences in radiation damage to carrier lifetimes in the neutral and depletion regions of InGaP and GaAs solar cells

Cite as: J. Appl. Phys. **132**, 115701 (2022); doi: 10.1063/5.0099106
Submitted: 15 May 2022 · Accepted: 19 August 2022 ·
Published Online: 15 September 2022

Tetsuya Nakamura,[1,a)] Mitsuru Imaizumi,[1] Shin-ichiro Sato,[2] Takeshi Ohshima,[2] Hidefumi Akiyama,[3,4] and Yoshitaka Okada[5,6]

AFFILIATIONS

[1]Japan Aerospace Exploration Agency, 2-1-1 Sengen, Tsukuba, Ibaraki 305-8505, Japan
[2]Quantum Beam Science Research Directorate, National Institutes for Quantum Science and Technology, 1223 Watanuki, Takasaki, Gunma 370-1292, Japan
[3]Institute for Solid State Physics, The University of Tokyo, 5-1-5 Kashiwanoha, Kashiwa, Chiba 277-0882, Japan
[4]AIST-UTokyo OPERANDO-OIL, The University of Tokyo, 5-1-5 Kashiwanoha, Kashiwa, Chiba 277-0882, Japan
[5]Research Center for Advanced Science and Technology, The University of Tokyo, 4-6-1 Komaba, Meguro-ku, Tokyo 153-8904, Japan
[6]Department of Advanced Interdisciplinary Studies, Graduate School of Engineering, The University of Tokyo, 4-6-1 Komaba, Meguro-ku, Tokyo 153-8904, Japan

Note: This paper is part of the Special Topic on Radiation Effects in Materials.
[a)]**Author to whom correspondence should be addressed:** nakamura.tetsuya@jaxa.jp

ABSTRACT

We investigated the radiation damage to carrier lifetimes in the neutral and depletion regions of the InGaP and GaAs subcells of an InGaP/GaAs/Ge triple-junction solar cell. It is difficult to clarify the degradation characteristics of the carrier lifetime in each region using the conventional analysis method (e.g., the dark current–voltage characteristic analysis), so we propose a novel method using the internal luminescence efficiency. The radiation damage coefficients for the carrier lifetimes in the neutral region of InGaP and GaAs subcells were two or three orders of magnitude larger than those in the depletion region. This result suggests that the effective radiation-induced defects in the regions, which significantly impact a solar cell's electrical characteristics, differ. This paper discusses the effective radiation-induced defects that contribute to the output degradation in each region. We compare the radiation damage coefficients for the carrier lifetimes obtained in our analysis, the product of the capture cross section, and the defect introduction coefficient of each defect reported in previous studies.

I. INTRODUCTION

InGaP/GaAs/Ge triple-junction (3J) solar cells[1] are widely used power sources for satellites due to their superior performance. Unfortunately, the output of a solar cell gradually decreases because of the high-energy electrons and protons in orbit that create radiation-induced defects. To improve the performance of solar cells at the end of life (EOL), it is important to understand the effects of radiation-induced defects on their electrical characteristics.

In general, the short-circuit current (Isc) is degraded by the radiation damage to the diffusion length in the neutral region. Previous studies have investigated this,[2,3] and this knowledge is reflected in the design of current 3J space solar cells, which show little Isc degradation caused by radiation. However, the output of the 3J solar cells cannot maintain the initial value in the orbital environment. The output of the 3J solar cells decreases due to the degradation of the open-circuit voltage (Voc).[4] This degradation is caused by a change in the non-radiative recombination lifetime due to radiation-induced defects. The challenge is to understand

radiation damage to the carrier lifetimes of the InGaP and GaAs subcells, which greatly affect the output of the 3J solar cells. Generally, a photo-generated carrier can recombine via defect levels in the solar cells' neutral and depletion regions. The effects of radiation damage to the carrier lifetime in the depletion region of GaAs solar cells have been reported.[5,6] However, to the best of our knowledge, no experiments on radiation damage to the carrier lifetime focusing on both the neutral and depletion regions have been reported. In order to obtain the carrier lifetimes in the neutral and depletion regions quantitatively and understand the radiation damage to the carrier lifetime in each region, a new analytical method is needed.

In this paper, we propose an analytical method for obtaining carrier lifetimes in the Shockley–Read–Hall (SRH) model via recombination centers[7,8] in the neutral and depletion regions. We expand the analytical method of internal luminescence efficiency (η_{int}) using the AB model[9] and apply it to 3J solar cells before and after irradiation.

A quantitative understanding of the radiation damage to the carrier lifetimes in the neutral and depletion regions of solar cells would be useful for improving radiation resistance and estimating the effective radiation-induced defects that affect the electrical characteristics in each region. Several reports describe the characteristics of radiation-induced defects, such as the defect level, the capture cross section, and the defect introduction coefficient by the deep level transient spectroscopy (DLTS) method.[10–13] Furthermore, the radiation-induced defects that behave as recombination centers in the depletion region of the GaAs solar cell have been reported.[5,6] However, the difference between such defects in the neutral and depletion regions remains unclear. In this paper, we discuss the effective radiation-induced defects contributing to the output degradation in the neutral and depletion regions and compare the experimentally obtained radiation damage coefficients for the carrier lifetimes in each region to the characteristics of radiation-induced defects clarified in previous studies.[10–13]

II. EXPERIMENTAL PROCEDURE

We employed commercial-grade bare InGaP/GaAs/Ge 3J solar cells,[14] which were $2 \times 2\,cm^2$. The 3J cells were irradiated with 1 MeV electrons using a Cockcroft–Walton accelerator and 3 MeV protons using a tandem accelerator at the National Institutes for Quantum Science and Technology. The 1 MeV electrons and 3 MeV protons created almost-uniform damage to InGaP and GaAs subcells. Irradiation fluence (ϕ) was 1×10^{13}, 2×10^{13} (3×10^{13} in total) and $7 \times 10^{13}\,cm^{-2}$ (1×10^{14} in total) for the 1 MeV electrons and 1×10^{10}, 2×10^{10} (3×10^{10} in total) and $7 \times 10^{10}\,cm^{-2}$ (1×10^{11} in total) for the 3 MeV protons. The fluence ranges were set, so the diffusion length was longer than the cell thickness to satisfy the assumptions of the analytical method described below. Cell current–voltage (IV) characteristics under simulated air mass zero light illumination (LIV) and absolute electroluminescence (EL) intensity[15] were measured before and after each irradiation. The external quantum efficiency (EQE) was measured only at the beginning of life (BOL) and EOL. Each measurement was performed at room temperature. We measured and analyzed the characteristics of the InGaP and GaAs subcells since these subcells greatly affect the output of the 3J solar cell. The external luminescence efficiency (η_{ext}), which is the ratio of the number of photons exiting the cell (P_{EL}) to the number of total recombination carriers (J/q), is given by $\eta_{ext} = qP_{EL}/J$, where q is the elementary charge and J is the injection current density. We calculated the average η_{int} of the whole subcell structure region ($\overline{\eta_{int}}$) using the following optical model:[16]

$$\eta_{ext} = \frac{\overline{\eta_{int}}\,\overline{P_{esc}}}{1 - \overline{\eta_{int}}\,\overline{P_{abs}}}. \tag{1}$$

Here, $\overline{P_{esc}}$ and $\overline{P_{abs}}$ are the average probabilities for a photon to escape from the front surface and be absorbed and collected as a photocurrent.

III. ANALYTICAL METHOD

This section describes the analytical model that we used to obtain the non-radiative recombination lifetimes in the neutral and depletion regions. We derived the non-radiative recombination lifetime in each region by analyzing the current dependence of the experimentally obtained $\overline{\eta_{int}}$. η_{int} can be expressed as follows, using the radiative recombination rate (U_{rad}) and the non-radiative recombination rate (U_{nr}):

$$\eta_{int} = \frac{U_{rad}}{U_{rad} + U_{nr}}. \tag{2}$$

Here, U_{rad} can be expressed using the bimolecular rate equation

$$U_{rad} = Bnp, \tag{3}$$

where B is the radiative recombination coefficient, n is the electron density, and p is the hole density. For non-radiative recombination, assuming that the SRH recombination via defect levels is dominant, U_{nr} during solar cell operation can be expressed as follows:[17,18]

$$U_{nr} = \frac{np - n_i^2}{\tau_{SRH}^p(n + n_1) + \tau_{SRH}^n(p + p_1)}, \tag{4}$$

$$n_1 = n_i \exp\left(\frac{E_t - E_i}{kT}\right), \tag{5}$$

$$p_1 = n_i \exp\left(\frac{E_i - E_t}{kT}\right). \tag{6}$$

Here, τ_{SRH}^p and τ_{SRH}^n are the SRH recombination lifetimes of a hole in the n layer and an electron in the p layer, respectively. n_i is the intrinsic carrier density, E_t is the level of the recombination centers, E_i is the intrinsic energy level, k is the Boltzmann constant, and T is the cell temperature. First, the internal luminescence efficiency of the neutral region (η_{int}^{neu}) is described using Eqs. (2)–(4). In this study, we focused on the recombination due to minority carrier traps in the p-type neutral region, which is the base layer of the 3J solar cells. The η_{int}^{neu} of the p-type neutral region ($\eta_{int}^{neu(p)}$) can

be expressed as follows, assuming that p is equal to the doping density (N_a) and N_a is sufficiently larger than n_i and p_1:

$$\eta_{\mathrm{int}}^{\mathrm{neu}(p)} \approx \frac{BN_a}{\frac{1}{\tau_{\mathrm{SRH}}^{\mathrm{neu}(n)}} + BN_a}. \tag{7}$$

Here, $\tau_{\mathrm{SRH}}^{\mathrm{neu}(n)}$ is the SRH recombination lifetime of an electron in the p-type neutral region. Equation (7) indicates that $\eta_{\mathrm{int}}^{\mathrm{neu}}$ is constant with respect to the minority carrier density (i.e., the injection current density). However, η_{int} in the depletion region ($\eta_{\mathrm{int}}^{\mathrm{dep}}$) can be written as shown in Eq. (8), assuming that n is equal to p and E_t is approximately equal to E_i,

$$\eta_{\mathrm{int}}^{\mathrm{dep}} \approx \frac{Bn^{\mathrm{dep}}}{\frac{1}{\tau_{\mathrm{SRH}}^{\mathrm{dep}(p)} + \tau_{\mathrm{SRH}}^{\mathrm{dep}(n)}} + Bn^{\mathrm{dep}}}, \tag{8}$$

$$n^{\mathrm{dep}} = n_i \exp\left(\frac{qV}{2kT}\right), \tag{9}$$

where n^{dep} is the n ($=p$) in the depletion region; $\tau_{\mathrm{SRH}}^{\mathrm{dep}(p)}$ and $\tau_{\mathrm{SRH}}^{\mathrm{dep}(n)}$ are the SRH recombination lifetimes of a hole and an electron in the depletion region, respectively; and V is the forward voltage. Equation (8) has also been derived for LEDs and is the basic equation of the so-called AB model.[19] Equation (8) indicates that $\eta_{\mathrm{int}}^{\mathrm{dep}}$ changes with respect to the injection current density.

To separate the experimentally obtained $\overline{\eta_{\mathrm{int}}}$ into $\eta_{\mathrm{int}}^{\mathrm{dep}}$ and $\eta_{\mathrm{int}}^{\mathrm{neu}}$, we defined the recombination ratio in the depletion region (r^{dep}) as $\Phi_{\mathrm{rec}}^{\mathrm{dep}}/\Phi_{\mathrm{rec}}$, and the recombination ratio in the neutral region (r^{neu}) as $\Phi_{\mathrm{rec}}^{\mathrm{neu}}/\Phi_{\mathrm{rec}}$, where Φ_{rec} is the number of total recombination carriers and $\Phi_{\mathrm{rec}}^{\mathrm{dep}}$ and $\Phi_{\mathrm{rec}}^{\mathrm{neu}}$ are the number of recombination carriers in the depletion and neutral regions, respectively. r^{neu} can be expressed as $1 - r^{\mathrm{dep}}$ since the non-radiation recombination is considered only for SRH recombination in this analysis. We assumed that the diffusion length was much longer than the cell thickness. In this case, all photocarriers generated by photon recycling are diffused and separated by the depletion region wherever they are re-absorbed. Therefore, even if re-emission and re-absorption are repeated, r^{dep} and r^{neu} are determined only by the minority carrier density after diffusion and separation (i.e., the injection current density). Based on this assumption, $\overline{\eta_{\mathrm{int}}}$ can be expressed as follows:

$$\overline{\eta_{\mathrm{int}}} = r^{\mathrm{dep}}\eta_{\mathrm{int}}^{\mathrm{dep}} + (1 - r^{\mathrm{dep}})\eta_{\mathrm{int}}^{\mathrm{neu}}. \tag{10}$$

Figure 1 shows the dependence of η_{int}, the forward voltage and r^{dep} on the injection current density of the solar cells. Note that Fig. 1 is a schematic diagram not measurement or simulation results. Using our assumptions, the dark IV (DIV) characteristics of solar cells can be described by the classical two-diode model,[4] which assumes that the diodes with the diode factors ($\mathrm{n_{diode}}$) of 1 and 2 are connected in parallel. The diode current density of $\mathrm{n_{diode}} = 1$ (J_1) denotes the current according to the radiative

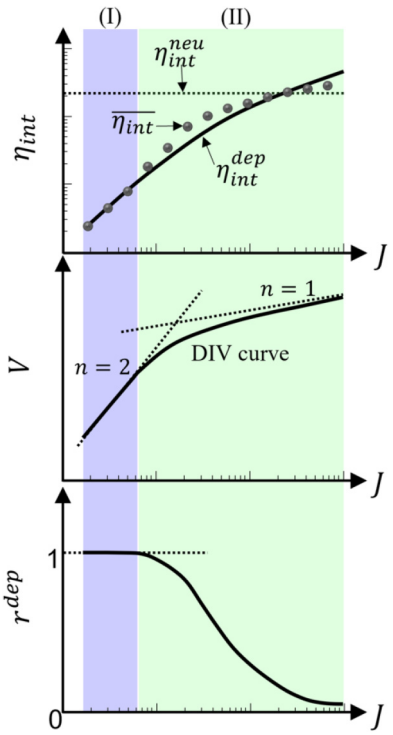

FIG. 1. Schematic diagrams of the dependence of η_{int}, the forward voltage, and r^{dep} on the injection current density of the solar cell. Note that these figures are not measurement or simulation results.

recombination in the whole region and the non-radiative recombination in the neutral region. $\mathrm{n_{diode}}$ for the non-radiative recombination in the depletion region can be expressed as 2, as shown in Eq. (9), since the SRH recombination current in the depletion region (J_2) is proportional to n^{dep}. In the low-current regime (regime I), r^{dep} is unity since all current flows into the diode with $\mathrm{n_{diode}} = 2$. Therefore, $\eta_{\mathrm{int}}^{\mathrm{dep}}$ and the SRH recombination lifetime in the depletion region can be obtained by fitting experimental $\overline{\eta_{\mathrm{int}}}$ data with Eq. (8) in regime I. In the high-current regime (regime II), $\overline{\eta_{\mathrm{int}}}$ changes according to Eq. (10) since current flows into both diodes with $\mathrm{n_{diode}} = 1$ and $\mathrm{n_{diode}} = 2$. It is possible to estimate $\eta_{\mathrm{int}}^{\mathrm{neu}}$, which is constant with respect to the injection current density, from the experimentally obtained $\overline{\eta_{\mathrm{int}}}$ and the analytically obtained $\eta_{\mathrm{int}}^{\mathrm{dep}}$ to satisfy $\eta_{\mathrm{int}}^{\mathrm{dep}} \le \overline{\eta_{\mathrm{int}}} \le \eta_{\mathrm{int}}^{\mathrm{neu}}$ or $\eta_{\mathrm{int}}^{\mathrm{neu}} \le \overline{\eta_{\mathrm{int}}} \le \eta_{\mathrm{int}}^{\mathrm{dep}}$.

IV. RESULTS

Figures 2(a) and 2(d) show the LIV curves before and after irradiation. The solid lines are the LIV curves of the 3J solar cells, and the dashed lines are the LIV curves of the InGaP and GaAs subcells calculated using the reciprocity relationship between EL and EQE[20] and the superposition principle by subtracting the Isc.[21,22] We used the initial EQE values to calculate the LIV characteristic of each subcell for each irradiation condition since there

was no significant change in EQE at BOL and EOL, as shown below. The Voc degradation (ΔVoc) of the 3J solar cell, the InGaP subcell, and the GaAs subcell due to 1 MeV electron irradiation ($\phi = 1 \times 10^{14}\,\mathrm{cm}^{-2}$ in total) were 178, 12, and 152 mV, respectively. In 3 MeV proton irradiation ($\phi = 1 \times 10^{11}\,\mathrm{cm}^{-2}$ in total), the ΔVoc of the 3J solar cell, the InGaP subcell, and the GaAs subcell were 224, 34, and 173 mV, respectively. Our result indicates that most of the voltage degradation by electron and proton irradiation in 3J solar cells is due to GaAs subcells. This is consistent with previous reports.[23–26] Figures 2(b) and 2(e) provide the EQE before and after irradiation. Considering the uncertainty of our EQE measurement system,[27] there was no significant change in EQE before and after irradiation. Figures 2(c) and 2(f) show the remaining factor (*RF*) of Isc, Voc, and maximum power point (Pmax). The solid lines in Figs. 2(c) and 2(f) are degradation curves from the following equation:

$$RF = 1 - C \log\left(1 + \frac{\phi}{\phi_x}\right). \tag{11}$$

Here, C and ϕ_x are coefficients computed from curve fitting. There was no change in Isc due to irradiation. These facts mean that under our experimental conditions, $\overline{P_{esc}}$ and $\overline{P_{abs}}$ did not change and only $\overline{\eta_{int}}$ was damaged. In addition, these results indicate that the assumption of the analytical model that the diffusion length is longer than the cell thickness is satisfied before and after irradiation.

Figures 3 and 4 plot the current dependence of η_{int} and the forward voltage before and after irradiations. The forward voltage was calculated from the reciprocity between EL and EQE.[20] The analysis used the initial values for EQE in all cases. In 1 MeV electron irradiation ($\phi = 1 \times 10^{14}\,\mathrm{cm}^{-2}$ in total), the experimentally obtained $\overline{\eta_{int}}$ at an injection current density of 20 mA/cm^2, which simulates the open-circuit condition under light irradiation,

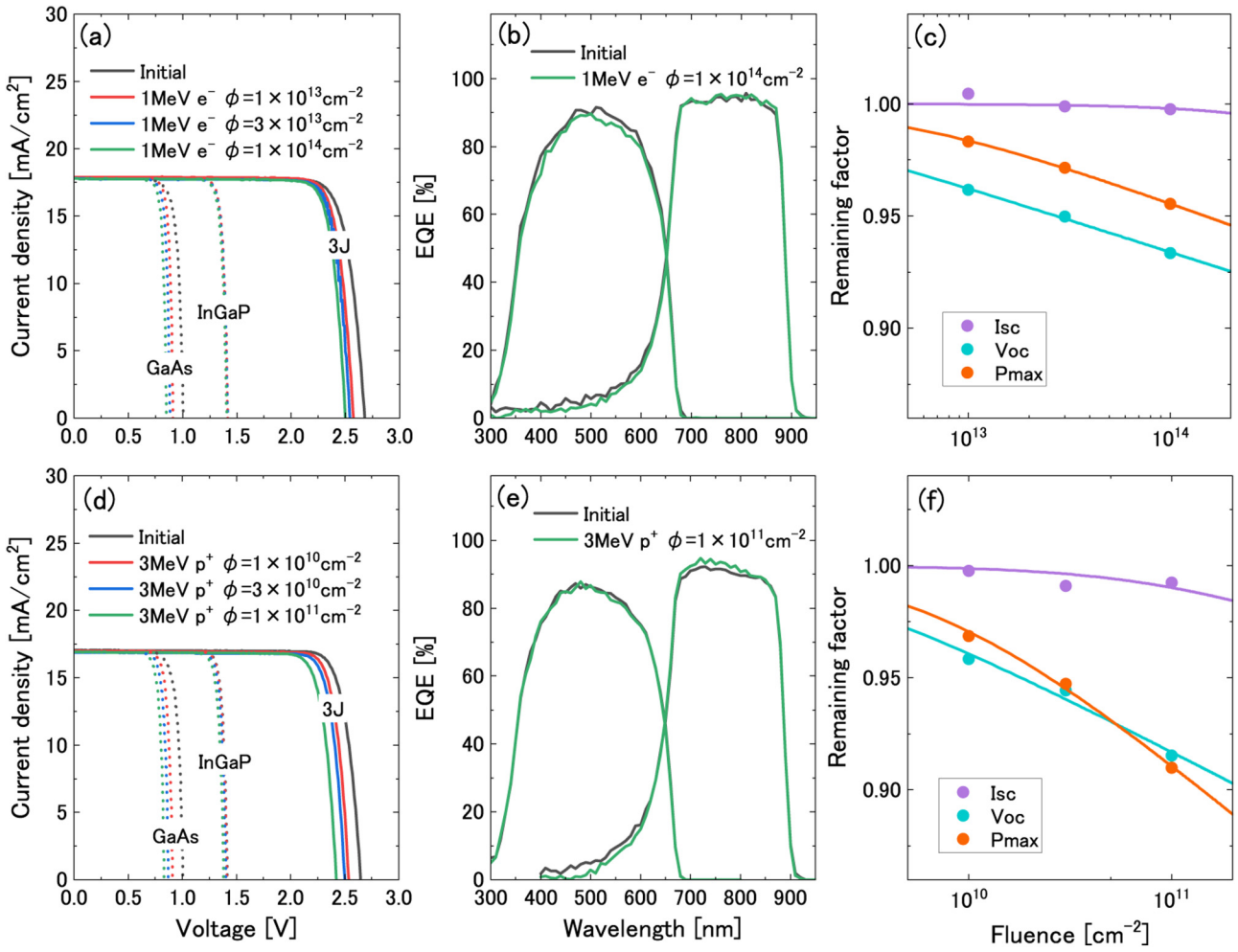

FIG. 2. (a)–(c) show LIV, EQE, and the remaining factor for 1 MeV electron irradiation. (d)–(f) for 3 MeV proton irradiation. In (a) and (d), solid lines are experimental data for the 3J solar cells, and dashed lines are data calculated for the subcells. In (c) and (f), solid lines are the fitting results using Eq. (11).

changed to approximately 2/3 and 1/180 in InGaP and GaAs subcells, respectively. In 3 MeV proton irradiation ($\phi = 1 \times 10^{11}$ cm^{-2} in total), $\overline{\eta_{\rm int}}$ at an injection current density of 20 mA/cm^2 changed to approximately 1/3 and 1/380 in InGaP and GaAs subcells, respectively. The degradation of $\overline{\eta_{\rm int}}$ of the GaAs subcells was much larger than that of the InGaP subcells. Furthermore, for GaAs subcells, the degradation of $\overline{\eta_{\rm int}}$ in the high-current regime (regime II) was larger than that in the low-current regime (regime I). The dashed lines in Figs. 3 and 4 are $\eta_{\rm int}^{\rm dep}$ to fit the experimentally obtained $\overline{\eta_{\rm int}}$ using Eq. (8) in the low-current regime (regime I) where the slopes of the IV curves of the solar cell and the diode with $n_{\rm diode} = 2$ are agreed well. The average SRH recombination lifetime in the depletion region $\overline{\left(\tau_{\rm SRH}^{{\rm dep}(p)} + \tau_{\rm SRH}^{{\rm dep}(n}\right)}$ was obtained as a fitting parameter. The results are shown in Tables I and II and Fig. 5. Here, $n^{\rm dep}$ of the two subcells were calculated from $n_i \exp(qV/2kT)$, where n_i is the intrinsic carrier density ($n_i^{\rm InGaP} = 1.2 \times 10^3$ cm^{-3}, $n_i^{\rm GaAs} = 1.79 \times 10^6$ cm^{-3}).[28] The B of the InGaP and GaAs subcells were 1.0×10^{-10} and 1.7×10^{-10} cm^3 s^{-1}, respectively.[29,30] The uncertainty analysis of the SRH recombination lifetime obtained from our measurement system has been reported previously.[9] The radiation damage coefficients[2] for the carrier lifetime (K_τ) were obtained by fitting the SRH recombination lifetimes with the following equation:

$$K_\tau = \frac{\tau_{\rm SRH\_irradiated}^{-1} - \tau_{\rm SRH\_initial}^{-1}}{\phi}. \quad (12)$$

K_τ can also be expressed by the product of the thermal velocity (υ) of minority carriers, the capture cross section (σ), and the

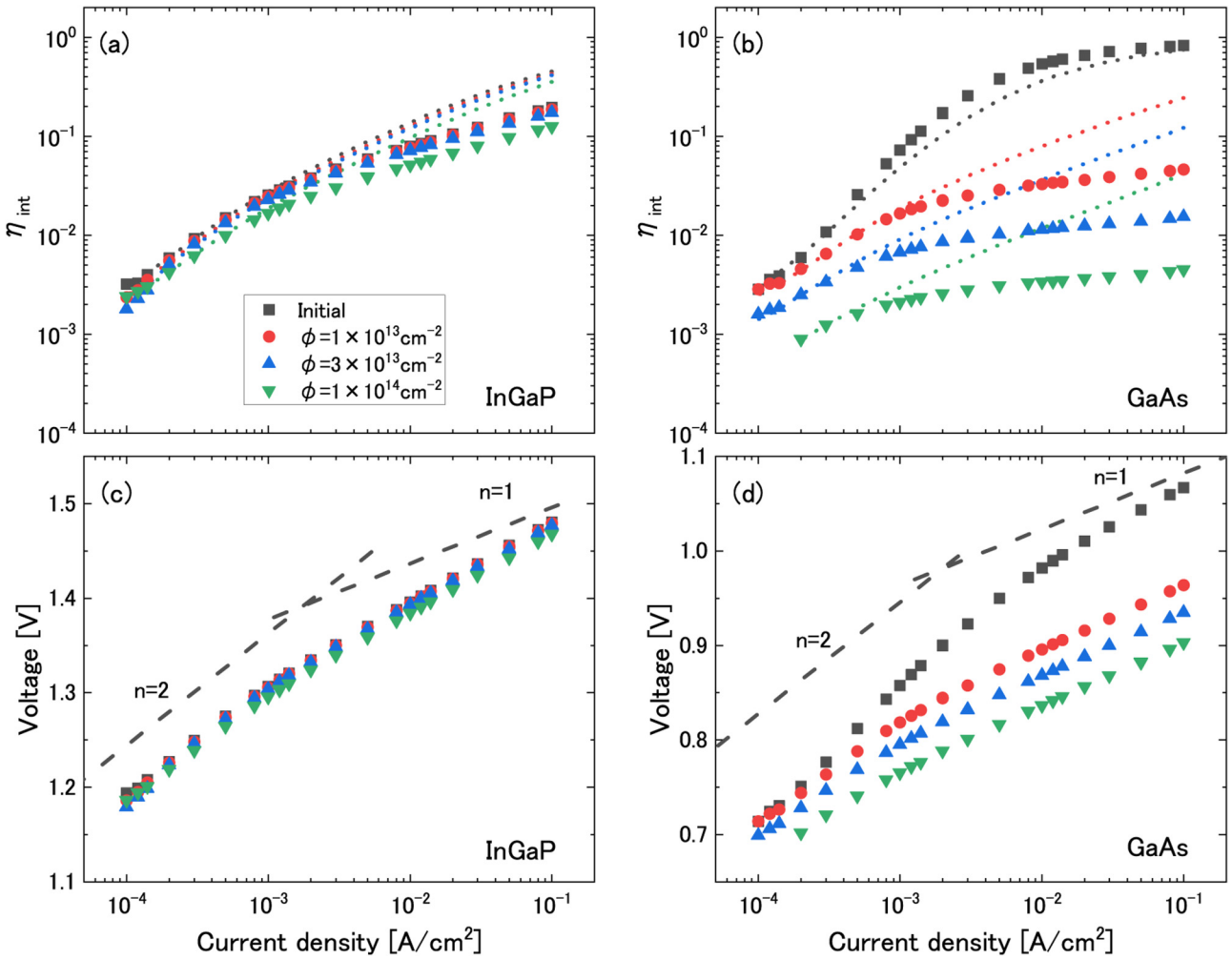

FIG. 3. Current dependence of $\eta_{\rm int}$ and forward voltage of InGaP and GaAs subcells before and after 1 MeV electron irradiation. In (a) and (b), dashed lines indicate results fitted to the experimentally obtained $\overline{\eta_{\rm int}}$ using Eq. (8) in the low-current regime. In (c) and (d), broken lines represent the slopes of the diode IV characteristics for $n_{\rm diode} = 1$ and $n_{\rm diode} = 2$.

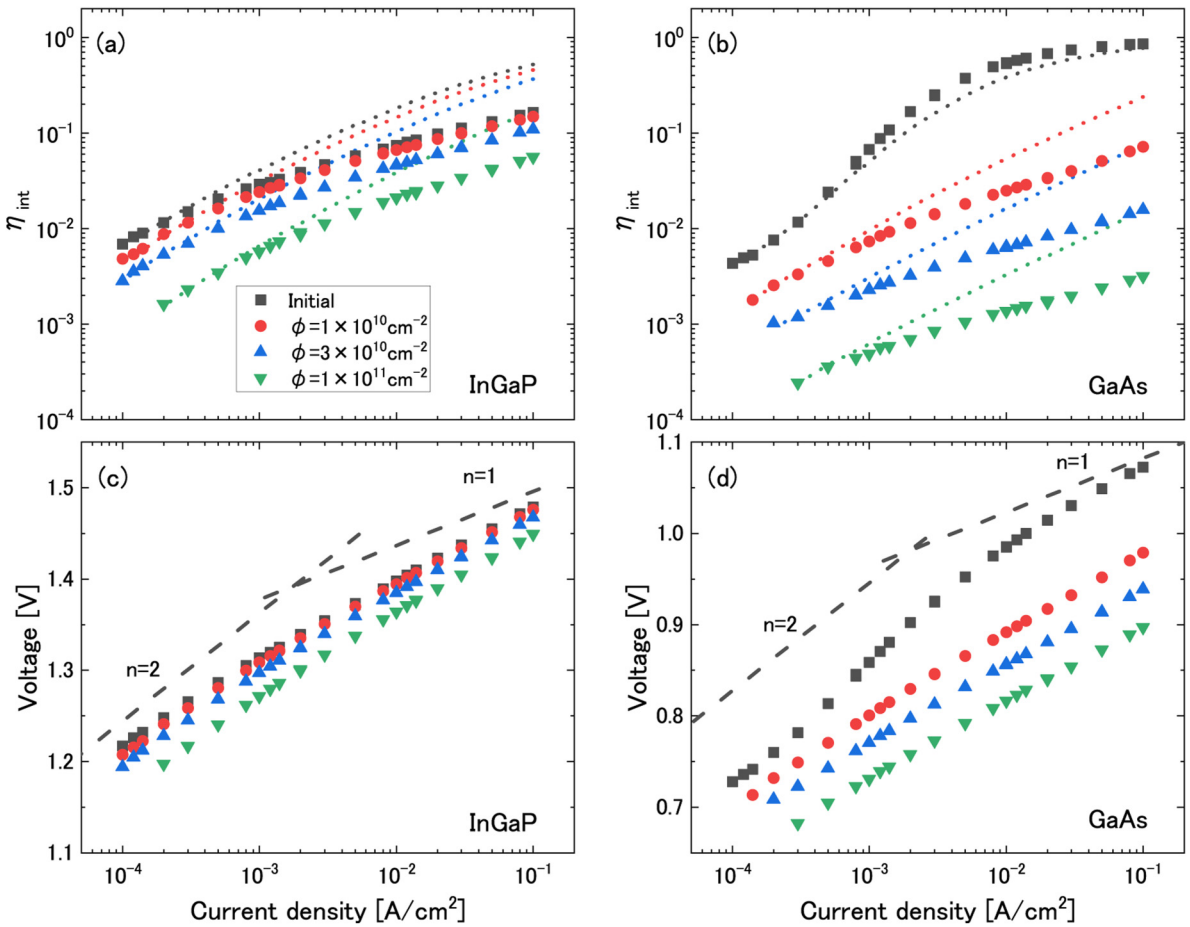

FIG. 4. Current dependence of η_{int} and forward voltage of InGaP and GaAs subcells before and after 3 MeV proton irradiation. In (a) and (b), the dashed lines indicate results fitted to the experimentally obtained $\overline{\eta_{int}}$ using Eq. (6) in the low-current regime. In (c) and (d), the broken lines represent the slopes of the diode IV characteristics of n_{diode} = 1 and n_{diode} = 2.

TABLE I. Obtained carrier lifetimes before and after 1 MeV electrons irradiation.

Subcell	Region	Initial	1×10^{13} cm^{-2}	3×10^{13} cm^{-2}	1×10^{14} cm^{-2}
InGaP	Depletion region	2.1×10^{-6} s	1.9×10^{-6} s	1.9×10^{-6} s	1.8×10^{-6} s
InGaP	Neutral region	3.0×10^{-8} s	3.8×10^{-8} s	3.6×10^{-8} s	1.7×10^{-8} s
GaAs	Depletion region	9.3×10^{-6} s	7.5×10^{-6} s	5.7×10^{-6} s	3.3×10^{-6} s
GaAs	Neutral region	1.5×10^{-5} s	2.2×10^{-8} s	7.0×10^{-9} s	2.4×10^{-9} s

TABLE II. Obtained carrier lifetimes before and after 3 MeV protons irradiation.

Subcell	Region	Initial	1×10^{10} cm^{-2}	3×10^{10} cm^{-2}	1×10^{11} cm^{-2}
InGaP	Depletion region	2.8×10^{-6} s	2.3×10^{-6} s	1.9×10^{-6} s	9.7×10^{-7} s
InGaP	Neutral region	1.5×10^{-8} s	1.7×10^{-8} s	1.0×10^{-8} s	5.0×10^{-9} s
GaAs	Depletion region	9.5×10^{-6} s	5.4×10^{-6} s	3.1×10^{-6} s	1.3×10^{-6} s
GaAs	Neutral region	1.3×10^{-5} s	6.9×10^{-9} s	2.3×10^{-9} s	6.5×10^{-10} s

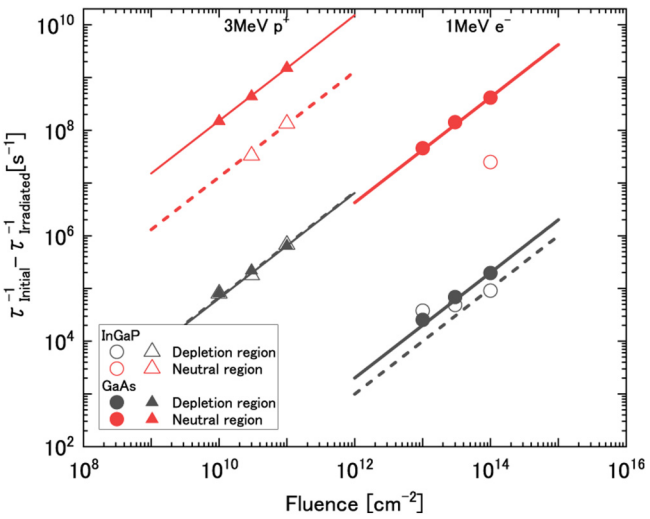

FIG. 5. Change in the carrier lifetime due to the electron and proton irradiation. Each line is a result of fitting using Eq. (12).

defect introduction coefficient (I) of radiation-induced defects, as shown below:

$$K_\tau = v\sigma I. \tag{13}$$

The obtained K_τ in the depletion region (K_τ^{dep}) of the InGaP and GaAs subcells are summarized in Table III. Although the change in $\eta_{\mathrm{int}}^{\mathrm{dep}}$ of the GaAs subcell was larger than that of the InGaP subcell, the K_τ^{dep} of the InGaP and GaAs subcells were almost the same in both electron and proton irradiation. Therefore, our result means that the degradation of the carrier lifetime by the electron and proton irradiation in InGaP and GaAs subcells are almost identical. However, ΔVoc in the GaAs subcell is much larger than that in the InGaP subcell. This is because the contribution of τ_{SRH} in the depletion region to the reverse saturation current density of the diode with $n_{\mathrm{diode}} = 2$ (J_{02}) differs between InGaP and GaAs subcells. J_{02} is proportional to τ_{SRH}^{-1} and n_i. Even if τ_{SRH}^{-1} changes by the same amount, the change in the J_{02} of the GaAs subcell is larger than that of the InGaP subcell since the n_i of GaAs is three orders of magnitude larger than the n_i of InGaP.

TABLE III. Analytical results of radiation damage coefficient.

		K_τ (s^{-1} cm^2)	
Subcell	Region	1 MeV e^-	3 MeV p^+
InGaP	Depletion region	9.96×10^{-10}	6.70×10^{-6}
InGaP	Neutral region	2.03×10^{-7}	1.30×10^{-3}
GaAs	Depletion region	2.00×10^{-9}	6.49×10^{-6}
GaAs	Neutral region	4.23×10^{-6}	1.52×10^{-2}

Next, K_τ in the neutral region (K_τ^{neu}) is introduced. The $\eta_{\mathrm{int}}^{\mathrm{neu}}$ of the GaAs subcell before irradiation was determined to be 0.9, which was the intersection of the experimentally obtained $\overline{\eta_{\mathrm{int}}}$ and the analytically obtained $\eta_{\mathrm{int}}^{\mathrm{dep}}$. In other cases, the maximum value of the $\eta_{\mathrm{int}}^{\mathrm{neu}}$, which satisfied Eq. (10), was derived from the boundary between regimes I and II as shown in Fig. 1. The SRH recombination lifetime was calculated using N_a and the value of B as shown in Tables I and II, and K_τ^{neu} was obtained by fitting the SRH recombination lifetime with Eq. (12), as shown in Table III. Since the lifetime of the InGaP subcell was not degraded at the low fluence of 1 MeV electrons, the K_τ^{neu} of the InGaP subcell was calculated only from the result of high fluence ($\phi = 1 \times 10^{14}$ cm^{-2} in total). We found that the K_τ^{neu} of the GaAs subcell was larger than the InGaP subcell. This fact is one of the reasons why the ΔVoc of the GaAs subcell is larger than that of the InGaP subcell except for the difference in the value of n_i. Furthermore, the analysis revealed that K_τ^{neu} was two or three orders of magnitude larger than K_τ^{dep} in each subcell. These results suggest that the effective radiation-induced defects that affect the electrical characteristics of each subcell differ in the neutral and depletion regions.

V. DISCUSSION

Previous studies have found σ and I of each radiation-induced defect formed in InGaP and GaAs by 1 MeV electron irradiation using the DLTS method.[10–13] By comparing K_τ/v obtained in this study and σI obtained in previous studies, we determined the radiation-induced defect that is dominant as an effective recombination center [Eq. (13)]. We calculated K_τ/v using the thermal velocities of electrons and holes, considering that the radiation-induced defects act as electron traps and hole traps, as shown in Table IV. Tables V and VI summarize σI reported in previous studies of the InGaP and GaAs, respectively.[10–13] "IE" and "E" labels indicate electron traps, and "H" indicates hole traps. First, we discuss the neutral region. The comparison suggests that IE1, IE2, and/or IE3[10] affect the electrical characteristics in the neutral region of the InGaP subcell. Furthermore, K_τ/v in the neutral region of the GaAs subcell corresponds to the σI of the E2 and/or E5 defects.[12] Our analysis of the neutral region assumes that minority carrier recombination in the p-type region is dominant. The results that the electron traps contribute to the electrical

TABLE IV. Estimated K_τ/v due to 1 MeV electron irradiation.

Subcell	Region	Assumed trap type	$\frac{K_\tau}{v}$ (cm)
InGaP	Depletion region	Electron trap	2.48×10^{-17}
InGaP	Depletion region	Hole trap	7.16×10^{-17}
InGaP	Neutral region	Electron trap	5.05×10^{-15}
InGaP	Neutral region	Hole trap	1.46×10^{-14}
GaAs	Depletion region	Electron trap	4.33×10^{-17}
GaAs	Depletion region	Hole trap	1.38×10^{-16}
GaAs	Neutral region	Electron trap	9.16×10^{-14}
GaAs	Neutral region	Hole trap	2.91×10^{-13}

TABLE V. σI of InGaP obtained from previous studies. A and B indicate $n_i \exp(|E_t - E_i|/kT)$ and $n_i \exp(qV/2kT)$. The forward voltage was 1.2 V.

Zaidi *et al.*[10]				Khan *et al.*[11]			
Labels	σI (cm)	$\lvert E_t - E_i\rvert$ (eV)	A/B	Labels	σI (cm)	$\lvert E_t - E_i\rvert$ (eV)	A/B
IE1	1.68×10^{-16}	0.82	5×10^{3}	E1	4.95×10^{-17}	0.66–0.75	1×10^{1}–3×10^{2}
IE2	1.90×10^{-16}	0.62	2	E2	4.62×10^{-18}	0.59	7×10^{-1}
IE3	3.51×10^{-14}	0.36	9×10^{-5}	E3	5.00×10^{-18}	0.23	6×10^{-7}
IE4	1.03×10^{-12}	0.30	7×10^{-6}	H1	6.20×10^{-19}	0.75	3×10^{2}
				H2	2.10×10^{-17}	0.40 – 0.45	4×10^{-4}–3×10^{-3}
				H3	2.08×10^{-17}	0.19	1×10^{-7}

performance are consistent with the assumption. If the hole traps of the n-type emitter layer contribute to the electrical characteristics, K_τ^{neu} is higher than this result since the emitter concentration is higher than the base concentration. However, there is no corresponding hole traps reported in previous studies. Next, K_τ/υ in the depletion region is described. We calculated the ratio of $n_i \exp(|E_t - E_i|/kT)(=A)$ and $n_i \exp(qV/2kT)(= B)$. If A/B in regime I is small enough, the assumption in Eq. (8) is satisfied and the comparison is valid. In the depletion region of the InGaP subcell, H2 and/or H3 defects[11] affect the electrical characteristics. Furthermore, K_τ/υ in the depletion region of the GaAs subcell corresponds to the σI of the H2 and/or H3 defects.[13] DIV analysis reports that the hole traps affect the electrical characteristics in the depletion region of the GaAs solar cell,[5] which is consistent with our analysis.

The radiation-induced defects that affect the electrical characteristics of a solar cell are determined by the carrier density distribution according to Eq. (4). In InGaP and GaAs subcells, our analysis suggests that hole traps and electron traps behave as effective recombination centers in the depletion and neutral regions, respectively.

VI. SUMMARY

This paper proposes an analytical method to obtain the SRH recombination lifetimes in the neutral and depletion regions of 3J solar cells. Using this method, we obtained the radiation damage coefficient for the carrier lifetime in each region of InGaP and GaAs subcells. By comparing the characteristics of radiation-induced defects quantified in previous studies, the effective defects that greatly affect the electrical characteristics of the solar cell were estimated. In InGaP and GaAs subcells, it was suggested that the hole and electron traps acted as effective recombination centers in depletion and neutral regions, respectively. In addition, we found that the radiation damage coefficient for the carrier lifetime of each region differs by two or three orders of magnitude. Our results clarified the radiation damage effects for the carrier lifetime of the InGaP and GaAs solar cells, which will be important for developing high radiation resistance in space solar cells.

ACKNOWLEDGMENTS

The authors thank the kind assistance of Jiro Harada, Mitsunobu Sugai, and Momoko Kohsaka of the AES Corporation for their help in characterizing the solar cells.

AUTHOR DECLARATIONS

Conflict of Interest

The authors have no conflicts to disclose.

Author Contributions

Tetsuya Nakamura: Conceptualization (equal); Data curation (equal); Formal analysis (equal); Funding acquisition (equal); Investigation (equal); Methodology (equal); Project administration (equal); Resources (equal); Supervision (equal); Validation (equal); Visualization (equal); Writing – original draft (equal); Writing – review & editing (equal). **Mitsuru Imaizumi**: Data curation (equal); Funding acquisition (equal); Investigation (equal); Methodology (equal); Project administration (equal); Resources

TABLE VI. σI of GaAs obtained from previous studies. A and B indicate $n_i \exp(|E_t - E_i|/kT)$ and $n_i \exp(qV/2kT)$. The forward voltage was 0.7 V.

Pons *et al.*[12]				Stievenard *et al.*[13]			
Labels	σI(cm)	$\lvert E_t - E_i\rvert$ (eV)	A/B	Labels	σI (cm)	$\lvert E_t - E_i\rvert$ (eV)	A/B
E1	3.30×10^{-15}	0.67	2×10^{5}	H1	1.20×10^{-16}	0.46	7×10^{1}
E2	1.80×10^{-13}	0.57	5×10^{3}	H2	4.40×10^{-16}	0.29	1×10^{-1}
E3	2.48×10^{-15}	0.41	1×10^{1}	H3	1.34×10^{-16}	0.17	9×10^{-4}
E4	2.48×10^{-15}	0.05	8×10^{-6}	H4	4.49×10^{-15}	0.08	3×10^{-5}
E5	1.90×10^{-13}	0.25	2×10^{-2}	H5	2.20×10^{-15}	0.14	3×10^{-4}

(equal); Supervision (equal); Validation (equal); Writing – review & editing (equal). **Shin-ichiro Sato**: Investigation (equal); Methodology (equal); Resources (equal); Writing – review & editing (equal). **Takeshi Ohshima**: Investigation (equal); Methodology (equal); Project administration (equal); Resources (equal); Supervision (equal); Writing – review & editing (equal). **Hidefumi Akiyama**: Conceptualization (equal); Formal analysis (equal); Methodology (equal); Resources (equal); Writing – review & editing (equal). **Yoshitaka Okada**: Conceptualization (equal); Methodology (equal); Writing – review & editing (equal).

DATA AVAILABILITY

The data that support the findings of this study are available from the corresponding author upon reasonable request.

REFERENCES

[1]D. C. Law, P. T. Chiu, C. M. Fetzer, M. Haddad, S. Mesropian, R. Cravens, P. H. Hebert, J. H. Ermer, and J. P. Krogen, in *Proceedings of 7th IEEE World Conference on Photovoltaic Energy Conversion (WCPEC), Waikoloa Village, HI* (IEEE, 2018), p. 3360.
[2]M. Yamaguchi and C. Amano, J. Appl. Phys. **57**, 537 (1985).
[3]D. Elfiky, M. Yamaguchi, T. Sasaki, M. Elnawawy, T. Eldesouky, and A. Ghitas, Jpn. J. Appl. Phys. **50**, 072301 (2011).
[4]R. Hoheisel, F. Dimroth, A. W. Bett, S. R. Messenger, P. P. Jenkins, and R. J. Walters, Sol. Energy Mater. Sol. Cells **108**, 235 (2013).
[5]C. Pellegrino, A. Gagliardi, and C. G. Zimmermann, Prog. Photovoltaics **27**(5), 379 (2019).
[6]C. Pellegrino, A. Gagliardi, and C. G. Zimmermann, J. Appl. Phys. **128**, 195701 (2020).
[7]W. Shockley and W. T. Read, Phys. Rev. **87**(5), 835 (1952).
[8]R. N. Hall, Phys. Rev. **87**(2), 387 (1952).
[9]T. Nakamura, M. Imaizumi, H. Akiyama, and Y. Okada, Prog. Photovoltaics Res. Appl. **28**(5), 417 (2020).
[10]M. A. Zaidi, M. Zazoui, and J. C. Bourgoin, J. Appl. Phys. **73**, 7229 (1993).
[11]A. Khan, M. Yamaguchi, J. C. Bourgoin, and T. Takamoto, J. Appl. Phys. **91**, 2391 (2002).
[12]D. Pons and J. C. Bourgoin, J. Phys. C: Solid State Phys. **18**, 3839 (1985).
[13]D. Stievenard and X. Boddaert, Phys. Rev. B **34**(6), 4048 (1986).
[14]G. S. Kinsey, R. R. King, K. M. Edmondson, A. P. Stavrides, H. Yoon, C. M. Fetzer, P. C. Colter, J. H. Ermer, M. S. Gillanders, P. Hebert, J. E. Granata, and N. H. Karam, in *Proceedings of 37th Intersociety Energy Conversion Engineering Conference (IECEC), Washington, DC, 29–31 July 2002* (IEEE, 2002), pp. 224–336.
[15]M. Yoshita, L. Zhu, C. Kim, H. Kubota, T. Nakamura, M. Imaizumi, Y. Kanemitsu, and H. Akiyama, in *Proceedings of 43rd IEEE Photovoltaic Specialists Conference, Portland, OR, 5–10 June 2016* (IEEE, 2016), pp. 3570–3573.
[16]M. A. Steiner, J. F. Geisz, I. Garcia, D. J. Friedman, A. Duda, and S. R. Kurtz, J. Appl. Phys. **113**, 123109 (2013).
[17]C.-T. Sah, R. N. Noyce, and W. Shockley, Proc. IRE **45**, 1228 (1957).
[18]R. Corkish and M. A. Green, J. Appl. Phys. **80**, 3083 (1996).
[19]J. I. Shim, D. P. Han, C. H. Oh, H. Jung, and D. S. Shin, J. Quantum Electron **54**(2), 8000106 (2018).
[20]U. Rau, Phys. Rev. B **76**(1), 085303 (2007).
[21]T. Kirchartz, U. Rau, M. Hermle, A. W. Bett, A. Helbig, and J. H. Werner, Appl. Phys. Lett. **92**, 123502 (2008).
[22]S. Roensch, R. Hoheisel, F. Dimroth, and A. W. Bett, Appl. Phys. Lett. **98**, 251113 (2011).
[23]T. Nakamura, M. Imaizumi, S-I Sato, and T. Ohshima, in *Proceedings of 38th IEEE Photovoltaic Specialist Conference (PVSC), Austin, TX* (IEEE, 2012), p. 2846.
[24]D. M. Tex, T. Nakamura, M. Imaizumi, T. Ohshima, and Y. Kanemitsu, Sci. Rep. **7**, 1985 (2017).
[25]L. Zhu, M. Yoshita, S. Chen, T. Nakamura, T. Mochizuki, C. Kim, M. Imaizumi, Y. Kanemitsu, and H. Akiyama, J. Photovoltaics **6**(3), 777 (2016).
[26]M. Imaizumi, T. Nakamura, T. Takamoto, T. Ohshima, and M. Tajima, Prog. Photovoltaics **25**(2), 161 (2017).
[27]T. Nakamura, L. Zhu, M. Yoshita, M. Imaizumi, H. Akiyama, and Y. Okada, in *Proceedings of 7th World Conference on Photovoltaic Energy Conversion, Waikoloa, HI, 10–15 June 2018* (IEEE, 2018), pp. 921–926.
[28]T. Oka, K. Ouchi, and K. Mochizuki, Jpn. J. Appl. Phys. **40**, 5221 (2001).
[29]U. Strauss, W. W. Ruhle, and H. J. Queisser, J. Appl. Phys. **75**, 8204 (1994).
[30]U. Strauss, W. W. Ruhle, and K. Kohler, Appl. Phys. Lett. **62**, 55 (1993).